J|A|C|S
ARTICLES
Published on Web 08/10/2006

Understanding the Role of Ti in Reversible Hydrogen Storage as Sodium Alanate: A Combined Experimental and Density Functional Theoretical Approach

Santanu Chaudhuri,[†] Jason Graetz,[‡] Alex Ignatov,[§] James J. Reilly,[‡] and James T. Muckerman*,[†]

Contribution from the Chemistry Department, Brookhaven National Laboratory, Upton, New York 11973-5000, Department of Energy, Science and Technology, Brookhaven National Laboratory, Upton, New York 11973, and National Synchrotron Light Source, Brookhaven National Laboratory, Upton, New York 11973

Received January 27, 2006; E-mail: muckerma@bnl.gov

Abstract: We report the results of an experimental and theoretical study of hydrogen storage in sodium alanate ($NaAlH_4$). Reversible hydrogen storage in this material is dependent on the presence of 2−4% Ti dopant. Our combined study shows that the role of Ti may be linked entirely to Ti-containing active catalytic sites in the metallic Al phase present in the dehydrogenated $NaAlH_4$. The EXAFS data presented here show that dehydrogenated samples contain a highly disordered distribution of Ti−Al distances with no long-range order beyond the second coordination sphere. We have used density functional theory techniques to calculate the chemical potential of possible Ti arrangements on an Al(001) surface for Ti coverages ranging from 0.125 to 0.5 monolayer (ML) and have identified those that can chemisorb molecular hydrogen via spontaneous or only moderately activated pathways. The chemisorption process exhibits a characteristic nodal symmetry property for the low-barrier sites: the incipient doped surface-H_2 adduct's highest occupied molecular orbital (HOMO) incorporates the σ^* antibonding molecular orbital of hydrogen, allowing the transfer of charge density from the surface to dissociate the molecular hydrogen. This work also proposes a plausible mechanism for the transport of an aluminum hydride species back into the NaH lattice that is supported by Car−Parrinello molecular dynamics (CPMD) simulations of the stability and mobility of aluminum clusters (alanes) on Al(001). As an experimental validation of the proposed role of titanium and the subsequent diffusion of alanes, we demonstrate experimentally that AlH_3 reacts with NaH to form $NaAlH_4$ without any requirement of a catalyst or hydrogen overpressure.

1. Introduction

The chemistry behind hydrogen storage is essentially the chemistry of the formation and decomposition of different hydrides under reversible conditions. The ease of formation of metal hydrides[1−4] from the native metallic state is dependent on the energies associated with the following key steps: (a) the chemisorption energy and activation barrier for the dissociation of molecular hydrogen and (b) the expansion and formation of the metal hydride lattice from the metal lattice. In regard to step (a), aluminum is one of the worst metals[5] in the periodic table for the dissociative chemisorption of molecular hydrogen to form hydride ions under moderate conditions. The chemisorption of molecular hydrogen by transition metals is often analyzed using the position of the center of the d-band with respect to the Fermi surface.[2,3] Aluminum, a member of group IIIA in the periodic table with an empty d-band, is not favorable[5] for a reaction with molecular hydrogen. The formation of aluminum hydride occurs at around 1100 °C or under very high pressures of H_2. As is the case with other group IIIA elements, once aluminum hydrides are formed, they are moderately stable[6] and exist in many crystallographically distinct phases.[7,8] At elevated temperatures, aluminum hydrides mostly dissociate into aluminum metal and hydrogen. The possibility of hydrogen storage in aluminum as a hydride may be an attractive idea,[9] but the chemistry of facile formation of the hydrides under near-ambient conditions is problematic for aluminum. An alternate route to aluminum hydrides is provided

[†] Chemistry Department.
[‡] Department of Energy, Science and Technology.
[§] National Synchrotron Light Source.

(1) Vehoff, H. Hydrogen in Metals III, Properties and Applications. *Hydrogen in Metals III*; Springer-Verlag: Berlin, 1997; Vol. 73, p 215.
(2) Smithson, H.; Marianetti, C. A.; Morgan, D.; Van der Ven, A.; Predith, A.; Ceder, G. *Phys. Rev. B: Condens. Matter Mater. Phys.* **2002**, *66*, 144107.
(3) Miwa, K.; Fukumoto, A. *Phys. Rev. B: Condens. Matter Mater. Phys.* **2002**, *65*, 155114.
(4) Alefeld, G.; Völkl, J. *Hydrogen in Metals II*; Springer: Berlin, 1978; Vol. 29, p 303.
(5) Hammer, B.; Jacobsen, K. W.; Norskov, J. K. *Phys. Rev. Lett.* **1992**, *69*, 1971.
(6) Wolverton, C.; Ozolins, V.; Asta, M. *Phys. Rev. B: Condens. Matter Mater. Phys.* **2004**, *69*, 144109.
(7) Brower, F. M.; Matzek, N. E.; Reigler, P. F.; Rinn, H. W.; Roberts, C. B.; Schmidt, D. L.; Snover, J. A.; Terada, K. *J. Am. Chem. Soc.* **1976**, *98*, 2450.
(8) Graetz, J.; Reilly, J. J. *J. Phys. Chem. B* **2005**, *109*, 22181.
(9) Sandrock, G.; Reilly, J.; Graetz, J.; Zhou, W. M.; Johnson, J.; Wegrzyn, J. *Appl. Phys. A: Mater. Sci. Process.* **2005**, *80*, 687.

10.1021/ja060437s CCC: $33.50

by materials that are members of the complex metal hydride family with the general formula $M_x(AlH_4)_y$ that are also called alanates. Their added stability compared to aluminum hydride comes from tetrahedrally coordinated aluminum atoms (AlH_4^-) shielded by countercations, which are mainly alkali metals. The chemistry of alanates has been known[10,11] for a long time. They are reactive and most of them dissociate to the respective alkali metal hydrides, aluminum, and hydrogen at or above room temperature. There is also a series of mixed alkali aluminum hydrides with the formula $A_xB_yAlH_6$ (known as elpasolites, and related to the A_3AlH_6 family called cryolites), with slightly lower hydrogen content that offers the possibility of finding the ideal structure−reactivity combination in complex metal hydrides.[12] In all cases, alanates have been considered promising aluminum-based materials with moderate hydrogen storage capacity, but the lack of efficient means of rehydrogenation has been a stumbling block to their development as hydrogen storage media. In this context, the discovery by Bogdanovic and Schwickardi[13] that the decomposition of $NaAlH_4$ can be made reversible at reasonable temperatures and pressures by adding titanium is understandably seminal but also puzzling. The puzzle lies in the fact that after thermal decomposition, the depleted material consists of fine grains of sodium hydride and aluminum, neither of which exhibits any reactivity toward molecular hydrogen under ambient conditions. Yet with Ti doping, the reverse of the following reaction occurs at a reasonably fast rate to form sodium alanate, a material with 5.6 wt. % of hydrogen.

$$NaAlH_4 \leftrightarrow \frac{1}{3}Na_3AlH_6 + \frac{2}{3}Al + H_2 \leftrightarrow NaH + Al + \frac{3}{2}H_2 \quad (1)$$

The rate of hydrogen generation can be controlled in the temperature range of 125−180 °C for the forward reaction. The reverse reaction is exothermic and (in the Ti-doped material) the fastest among other complex metal hydrides. The reverse reaction is typically run in the temperature range of 140−200 °C and under a slight overpressure (5−15 MPa) of hydrogen. The question has remained: What has changed due to this 2−4% Ti doping to so drastically increase the reactivity of this nearly inert metal toward molecular hydrogen? In our previous work,[14] we identified an active Al−Ti site that demonstrated that spontaneous hydrogen chemisorption was possible on an aluminum surface. There are other reported theoretical studies[15,16] that attempt to explain why the presence of titanium can make the forward (decomposition) reaction of the alanate easier. Because a number of studies suggest that the Ti dopant is associated with Al, and there is little experimental evidence that titanium can be incorporated into the sodium alanate lattice, the calculations presented here assume the Ti to be concentrated in the Al phase.

In this study, we extend and combine our previous theoretical[14] and experimental results[17,18] to investigate the atomic-level mechanism responsible for reversible hydrogenation−dehydrogenation in Ti-doped sodium alanate. This investigation was performed using extended X-ray absorption fine structure (EXAFS), X-ray diffraction (XRD), and density functional theoretical calculations. These results support a growing consensus in the community that the activity is due to the presence of 2−4 mol % titanium associated exclusively with the metallic aluminum phase, and that the location of titanium atoms does not change with hydrogenation−dehydrogenation cycles even though the amount of metallic aluminum does. Not all the aluminum in the hydrogen-depleted material reacts to reform the $NaAlH_4$ starting material, leaving the titanium concentrated in the remaining aluminum phase. This is suggestive[17,18] of the formation of a stable surface alloy phase of titanium and aluminum similar to $TiAl_3$ and a considerable energy cost associated with dismantling such arrangements during the forward and reverse reactions.

The chemisorption of molecular hydrogen on an Al surface activated by Ti doping has been proposed as the critical first step in hydrogen storage in alanates.[14] Several subsequent steps are required for an aluminum hydride species to be transported into the NaH lattice to form the intermediate cryolite phase, Na_3AlH_6. Alane (AlH_3 and its oligomers) formation has been proposed as a mobile aluminum hydride species. Motivated by related experimental evidence presented elsewhere,[19−21] quantum-force DFT molecular dynamics (MD) studies have been carried out and are used to explore a plausible mechanism by which the alane species (AlH_x) can transport hydrogen and aluminum together to the NaH lattice and form Na_3AlH_6.

2. Methods

EXAFS and Sample Preparation. X-ray absorption studies of the Ti *K*-edge were performed on hydrogenated and dehydrogenated sodium alanate doped with 2 and 4 mol % $TiCl_3$. The samples were prepared by mechanically alloying $NaAlH_4$ (Alfa Chem. Co. 95%) with $TiCl_3$ (Aldrich 99%) using a Fritsch Pulverizette 6 planetary mill. Approximately 1.2 g of the mixed powders were milled in a 0.25 L tungsten carbide bowl using seven 15-mm diameter tungsten carbide balls (~26 g each) for 1.5 h under an Ar atmosphere. The mechanochemical preparation and subsequent cycling of $NaAlH_4$ and $TiCl_3$ leads to the formation of NaCl and excess Al.[17,22] For each Ti concentration, samples were taken immediately after balling and after cycling four times through the hydrogenation/dehydrogenation steps of reaction 1. Of the cycled material, one sample was prepared fully hydrogenated ($NaAlH_4$) and another completely dehydrogenated (NaH + Al). All powders were sieved through 325 mesh (44 μm) and brushed onto Kapton tape, whereas the ductile alloy of $Ti_{0.08}Al_{0.92}$ was pressed into a thin pellet.

X-ray absorption spectra were acquired at the National Synchrotron Light Source (NSLS) of Brookhaven National Laboratory. The spectra were collected on beamline X-19A using a Si(111) double crystal monochromator and recorded in fluorescence yield. A passivated implanted planar silicon detector was used for the reasonably concentrated samples, whereas spectra from samples with a dilute Ti concentration were acquired with a 13-element Ge detector (Canberra). Due to the small Ti concentrations, the near-edge spectra were not

(10) Kondoh, H.; Hara, M.; Domen, K.; Nozoye, H. *Surf. Sci.* **1993**, *287*, 74.
(11) Hara, M.; Domen, K.; Onishi, T.; Nozoye, H. *J. Phys. Chem.* **1991**, *95*, 6.
(12) Graetz, J.; Lee, Y.; Reilly, J. J.; Park, S.; Vogt, T. *Phys. Rev. B* **2005**, *71*, 184115.
(13) Bogdanovic, B.; Schwickardi, M. *J. Alloys Compd.* **1997**, *253*, 1.
(14) Chaudhuri, S.; Muckerman, J. T. *J. Phys. Chem. B* **2005**, *109*, 6952.
(15) Iniguez, J.; Yildirim, T.; Udovic, T. J.; Sulic, M.; Jensen, C. M. *Phys. Rev. B: Condens. Matter Mater. Phys.* **2004**, *70*, 060101.
(16) Iniguez, J.; Yildirim, T. *Appl. Phys. Lett.* **2005**, *86*, 103109.
(17) Graetz, J.; Ignatov, A. Y.; Tyson, T. A.; Reilly, J. J.; Johnson, J. *Mater. Res. Soc. Conf. Proc.* **2005**, *837*.
(18) Graetz, J.; Reilly, J. J.; Johnson, J.; Ignatov, A. Y.; Tyson, T. A. *Appl. Phys. Lett.* **2004**, *85*, 5000.
(19) Kurth, F. A.; Eberlein, R. A.; Schnockel, H.; Downs, A. J.; Pulham, C. R. *J. Chem. Soc. Chem. Commun.* **1993**, 1302.
(20) Raston, C. L. *J. Organomet. Chem.* **1994**, *475*, 15.
(21) Go, E. P.; Thuermer, K.; Reutt-Robey, J. E. *Surf. Sci.* **1999**, *437*, 377.
(22) Majzoub, E. H.; Gross, K. J. *J. Alloys Compd.* **2003**, *363*, 356.

corrected for "self-absorption." All samples were kept at room temperature, and air-sensitive samples were measured in a sealed sample holder under Ar gas.

Theoretical Background. Pseudopotential DFT Calculations. This study used the density functional theory program CASTEP[23] for most of the calculations presented. The generalized gradient approximation (GGA) with a plane-wave pseudopotential (PWPSP) basis and the RPBE[24] exchange-correlation functional were employed in the calculations. Ultrasoft pseudopotentials were used to replace the core electrons. All the geometry optimization calculations were performed with a 270 eV energy cutoff with the convergence criterion set at 2×10^{-5} eV/atom. The results were then tested for convergence at a finer k-mesh and much higher energy cutoff values to verify the minima and to determine any dependence on k-spacing. Mulliken charge and overlap population analyses were performed using the pseudo-atomic wave functions. In all cases reported here, a spin-restricted (spin-unpolarized) approach was employed with no net charge on the unit cell. Band structures and partial densities of states (DOS) of the different surfaces were calculated for Γ points only. We also performed spin-polarized calculations but the results are not presented here because the Ti atoms have no net spin and the energy gain is negligible compared to the gain in energy due to the doubling of the number of basis functions alone. We have calculated the barriers of hydrogen dissociation on different configurations of Ti-doped Al(001) surfaces using the LST/QST (linear synchronous transit/quadratic synchronous transit) technique.[25]

All-Electron DFT using Atomic Orbital Basis Sets. Density functional theory as implemented in the DMol3 program[26,27] was used to inspect the orbitals involved in the bonding. This allowed us to replace the core treatment and plane-wave basis set of CASTEP by all-electron atomic basis sets. Our calculation included 454 atomic orbitals and 332 total electrons. A particular variation of numerical atomic basis sets called DNP (double numerical plus polarization) was employed. It includes a double-ζ basis for the valence orbitals along with polarization p-functions on all hydrogen atoms and polarization d-functions on all aluminum atoms (plus a set of 4p functions but not 4f functions on titanium atoms). The same exchange-correlation functional (RPBE) was used as in the CASTEP calculations. Only the results addressing molecular orbital interactions were calculated by this all-electron method.

Density Functional Molecular Dynamics Simulation of Surface Diffusion. Periodic density functional molecular dynamics (DFT-MD) simulations were performed using CASTEP to understand the temperature effect on hydrogen atom diffusion on the doped aluminum surface following chemisorption. The time-step used for the simulations was 2×10^{-15} s, and results from 1-ps simulations are reported here. Each simulation step performs an extended Lagrangian classical molecular dynamics (MD) step based on the forces calculated from the PWP DFT technique described above. A significant speedup is possible in this otherwise costly method by using a variant of the wave function and density extrapolation scheme originally proposed by Arias et al.[28] The electrons were kept on the Born−Oppenheimer surface by explicitly minimizing the electronic part after each MD step. An NVT (constant volume and temperature) ensemble dynamics was employed with Nosé-Hoover-type thermostats of chain length 6. This approach is preferred over NPT (constant pressure and temperature) ensemble dynamics in the current calculations because of the lack of numerical stability of NPT at a solid-phase/gas-phase interface.

Car−Parinello Dynamics. For the molecular dynamics simulation of the diffusion of alane species, Car−Parinello molecular dynamics was selected as the most efficient tool. Different stable gas-phase alane clusters and their diffusion on an Al metal surface were investigated. A three-atomic-layer thick periodic unit, consisting of 96 aluminum atoms in the 2D periodic unit, represents an Al(001) surface in this study. Different stable gas-phase alane clusters were tested on this model surface for surface diffusion and dissociation properties at different temperatures. The clusters tested were AlH_3, Al_2H_6, and Al_3H_9. The system size was thus 100−108 atoms (96 Al-atom periodic Al(001) surface plus 4, 8, or 12 atoms of the cluster) depending on the size of the alane cluster tested. The gas-phase structure of each cluster was first optimized using the same DNP basis sets described above. Then each cluster was optimized on the Al(001) support. Car−Parinello MD (CPMD) NVT simulations[29] at 200 and 400 K were performed with Nosé−Hoover type thermostats and using GGA-PBE[30] functionals. Each simulation step was 0.2 fs for an accurate description of the wave function and better performance of the CPMD algorithm under nearly Born−Oppenheimer conditions.

Building Surfaces and Testing Reactivity The Al(001) 2×2 surface used in all the calculations consists of an infinitely periodic surface composed of these 2×2 repeating units containing 24 atoms in the periodic unit cell. We have chosen Al(001) for our model Al surface for three reasons: (1) the chemisorption of hydrogen *atoms* is energetically most favorable[31] on an Al(001) surface; (2) Ti forms segregated regions of stable surface alloys on Al(001),[32,33] which should be more favorable compared to a subsurface alloy for promoting reaction, and experimental indications point to localized Ti−Al phases; and (3) hydrogen also binds strongly to microfacets (similar to the environment modeled in this work) in Al(111) steps making {001} a ubiquitous face for hydrogen absorption. The exposed surfaces in all cases were given a layer of vacuum as large as 25−30 Å to avoid interactions with its periodic image in the vertical direction. Our experience suggests that the above-mentioned separation and relaxation of two surface layers of atoms followed by a few fixed layers of Al atoms are the minimum requirement for achieving consistent energies and other ground-state properties. In this particular case, increasing the number of fixed Al layers does not have any significant effect apart from increasing the computational cost. Different orientations of an approaching hydrogen molecule have been considered, and the hydrogen molecule has been placed just above the surface at a distance that represents the sum of van der Waals radii of the respective atoms.

3. Results

Possible Ti Arrangements. Understanding the probable locations of the titanium atoms in the metallic aluminum phase is the key to understanding the catalytic role of the dopant and the subsequent steps in the hydrogenation reaction. However, the number of possible Ti configurations is enormous. A sensible approach is to first evaluate the reactivity of possible arrangements in the Al(001) surface, i.e., among the many possible aluminum surfaces that can exist in a disordered aluminum grain, concentrating on the ones with the largest affinity for H atoms. Also, the Ti coverage is dependent on the available surface area of the phase. The depleted material is generated after desorption of the hydrogen, which leaves the material in a spongy and high-surface-area state. The particle sizes are extremely small (as

(23) Segall, M. D.; Lindan, P. J. D.; Probert, M. J.; Pickard, C. J.; Hasnip, P. J.; Clark, S. J.; Payne, M. C. *J. Phys.-Condens. Mater.* **2002**, *14*, 2717.
(24) Hammer, B.; Hansen, L. B.; Norskov, J. K. *Phys. Rev. B: Condens. Matter Mater. Phys.* **1999**, *59*, 7413.
(25) Halgren, T. A.; Lipscomb, W. N. *Chem. Phys. Lett.* **1977**, *49*, 225.
(26) Delley, B. *J. Chem. Phys.* **1990**, *92*, 508.
(27) Delley, B. *J. Chem. Phys.* **2000**, *113*, 7756.
(28) Arias, T. A.; Payne, M. C.; Joannopoulos, J. D. *Phys. Rev. Lett.* **1992**, *69*, 1077.
(29) *CPMD V3.9*, IBM Corp: MPI fuer Festkoerperforschung Stuttgart, Copyright IBM Corp 1990−2004.
(30) Perdew, J. P.; Burke, K.; Ernzerhof, M. *Phys. Rev. Lett.* **1996**, *77*, 3865.
(31) Stumpf, R. *Phys. Rev. Lett.* **1997**, *78*, 4454.
(32) Kim, Y. W.; White, G. A.; Shivaparan, N. R.; Teter, M. A.; Smith, R. J. *Surf. Rev. Lett.* **1999**, *6*, 775.
(33) Saleh, A. A.; Shutthanandan, V.; Shivaparan, N. R.; Smith, R. J.; Tran, T. T.; Chambers, S. A. *Phys. Rev. B: Condens. Matter Mater. Phys.* **1997**, *56*, 9841.

small as 10 nm[34]), making a surface-segregated 2−4% Ti concentration correspond to a submonolayer coverage. In a hypothetical model of a spherical aluminum particle with a 20 nm diameter, even with the assumption that an entire 2 mol % pool of titanium atoms surface segregates, the titanium surface coverage is ~0.3 monolayer (ML). Given the expected concentration fluctuations during the hydrogenation−dehydrogenation cycles, the titanium coverage explored here is in the range of 0.125 to 0.5 ML in the aluminum phase.

To enable the comparison of the stability of arrangements of dopant Ti atoms in Al surfaces *at different coverages*, it is necessary to define the free energy (chemical potential) of each such arrangement relative to the most stable state of the system, which is taken as a reference state. For systems with the same number of Ti and Al atoms, one could simply compare the total energies, but not all the various model systems have the same composition. Moreover, the most stable state of the actual system is somewhat ambiguous. Because Ti does not form a solid solution in Al, and the dilute composition $Ti_{0.08}Al_{0.92}$ used for EXAFS calibration is a two-phase mixture with regions of $TiAl_3$ embedded within the bulk Al, the most appropriate choice of reference state is the most stable surface termination of the $TiAl_3$ alloy. Below, we discuss two methods of calculating the relative stability of different model sites.

Method 1: Because Ti is the minority component in the systems, the "traditional" approach is to use it as the indicator of the chemical potential of each *system*. For a supercell containing N atoms of which *n* are Ti atoms, we can express the chemical potential (neglecting small corrections for zero-point energy, pressure volume work, thermal energy, and entropy of mixing) of the Ti atoms as $E_{Ti} = [E_{system} - (N - n)E_{Al}]/n$ where E_{system} is the computed total electronic energy of the system, and E_{Al} is the computed electronic energy per atom in bulk Al. The justification for using the bulk Al value is that the vast majority of atoms in a physical sample are Al surrounded by other Al atoms. To put these free energies on a scale in which the leading figures are significant, we subtract the computed energy of a free Ti atom to obtain the binding energy per Ti atom, E_b. If the same calculation is performed with respect to a "per Al atom" scale, the trend we discuss later is the same but the magnitude is smaller as we are dividing the energy by the number of the higher concentration species. This procedure becomes questionable when applied to nearly equal mixtures of the two components, e.g., in the $TiAl_3$ alloy, but the "eV/Ti atom" scale is nevertheless an estimator for the overall chemical potential, and its magnitude is more faithful to the effect of Ti as a dilute species.

Method 2: As an alternative to the traditional approach described above, we also calculate the chemical potential of 24-atom systems (the size of our supercell) plus 6 free atoms drawn from a pool of 30 free atoms consisting of 24 Al atoms and 6 Ti atoms. Then we calculate $[(E_{system} + (6 - n)E_{Ti} + nE_{Al}) - (24E_{Al} + 6E_{Ti})]/30$ as the "per atom" binding energy. Here, E_{Al} and E_{Ti} are in this case the electronic energies of the respective free atoms. The 6 Ti atoms are required to calculate the energy of the 24-atom supercell for the $TiAl_3$ alloy. Subtracting the energies of the 30 free atoms cancels the contribution to the system energy from the 6 atoms not placed in the supercell, so our binding energy per atom differs from that of the supercell alone only because we divide the total binding energy by 30 instead of 24. The calculated results using this method for the various model systems are plotted in Figure S1 in the Supporting Information. The calculated values are valid for the 24-atom models we employ, but these models are intended to represent the surface region of samples that are much deeper than the three explicit layers we treat (which were sufficient to converge the energy per atom of pure Al). With an increasing number of Al layers, the binding energy calculated by this method would change and approach the value of the binding energy for pure Al(001) (−3.5812 eV/atom). That is not an intended consequence for a study of surface coverage effects. In such a case, we would also need to change the size of the pool from the current 30 atoms to a larger number to evaluate the chemical potential of all possible arrangements. No such problem exists for the application of Method 2 to bulk systems, e.g., $TiAl_3$.

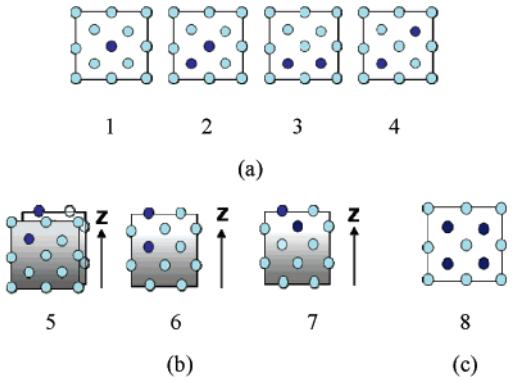

Figure 1. Schematic presentation of different titanium (dark blue circle) arrangements studied on a Al(001) surface: (a) ≤0.25 ML Ti coverage on the surface and two immediate subsurface layers; (b) the vertical surface−subsurface arrangement of 0.25 ML Ti doped samples; and (c) the 0.5 ML Ti coverage arrangement.

Several possible arrangements of Ti atoms in the Al(001) surface and subsurface layers were investigated using the pseudopotential DFT methods described above. The energies calculated are then compared using the scales of chemical potential presented above. Only the surface and one subsurface layers are considered. This is because the catalytic hydrogen chemisorption process requires the Ti atoms (or their effect on surface Al atoms) to be accessible to the molecular hydrogen. Also, based on the experimental electron microscopic and thin-film studies[33] together with the EXAFS results presented in this paper, it is clear that the Ti atoms are present in an under-coordinated environment exclusively in the aluminum phase. Figure 1 shows several such arrangements of Ti atoms on the 2 × 2 surface unit cell of Al(001) consistent with a 0.125−0.5 ML Ti surface coverage. The energies are calculated for the surface and subsurface arrangements. The general trend shows that the first subsurface layer is energetically more favorable for Ti atoms compared to the surface layer. In this paper, the number below the model in Figure 1 refers to a particular arrangement, e.g., Model 1 to represent one titanium in the 2 × 2 supercell. Some of the calculated chemical potential values for the different 0.25 and 0.5 ML arrangements are tabulated in Table 1 and are compared to various possible choices for a reference state in Figure 2.

(34) Felderhoff, M.; Klementiev, K.; Grunert, W.; Spliethoff, B.; Tesche, B.; von Colbe, J. M. B.; Bogdanovic, B.; Hartel, M.; Pommerin, A.; Schuth, F.; Weidenthaler, C. *Phys. Chem. Chem. Phys.* **2004**, *6*, 4369.

Table 1. Energies, or Chemical Potentials, (in eV/Ti atom)[a] Using Method 1 of a Few Relevant Ti Arrangements (~0.25−0.5 ML Coverage) on the Al(001) Surface[b]

				
	Model 2[c]	Model 3	Model 4[d]	Model 8
E_b (surface)	−3.46 (−2.85)	−3.80 (−2.87)	−4.85 (−2.94)	−5.89 (−3.16)
E_b (subsurface)	−4.11 (−2.89)	−4.20 (−2.89)	−5.28 (−2.95)	−6.46 (−3.24)

[a] All the energies are quoted in eV/atom. The following values were used to calculate the chemical potentials: (a) free Ti atom, E_∞= −1599.46 eV/atom; (b) bulk Ti, −1606.03 eV/atom (E_b= −6.57 eV); (c) $TiAl_3$_001, −1606.39 eV/atom (E_b= −6.93 eV); (d) $TiAl_3$ bulk, −1608.01 eV/atom (E_b= −8.55 eV); (e) Free Al, E_∞ = −53.66 eV; (f) Bulk Al, E_0= −57.23 eV (E_b = −3.57 eV). [b] Shown schematically in Figure 1 as Models 2, 3, 4, and 8. [c] The chemical potential calculated using Method 2 for the different model sites is quoted in parentheses (eV/atom) showing that the order of relative stability does not change. [d] The surface value for Model 4 corresponds to the reconstructed surface.

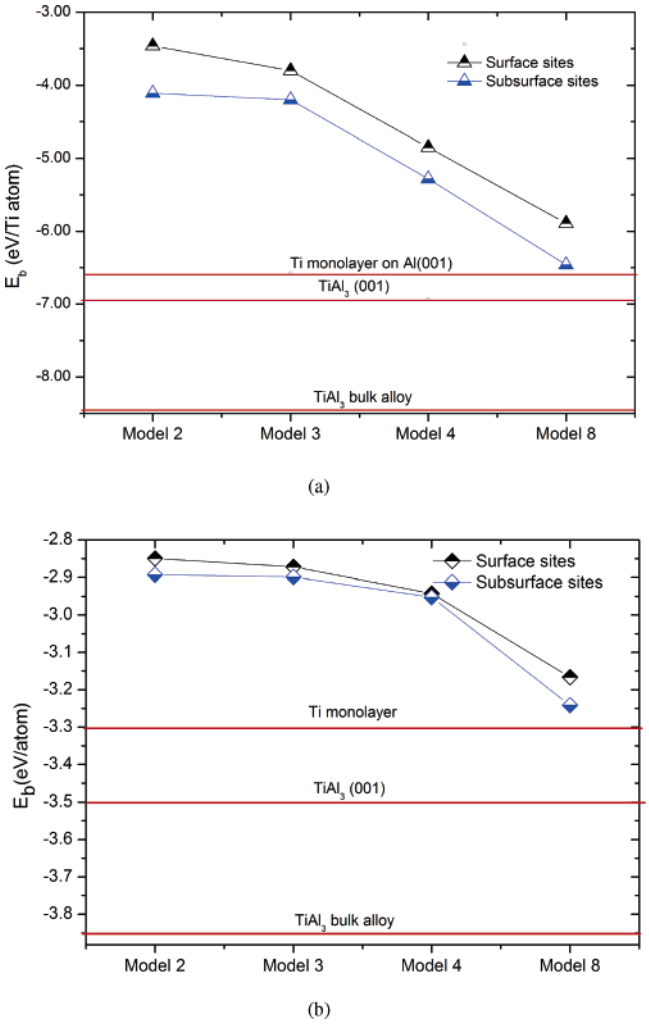

Figure 2. Energies, or chemical potentials, for different sites calculated using Method 1 and Method 2 that are tabulated in Table 1 are plotted in (a) and (b), respectively. The red lines provide the chemical potentials of candidate reference states calculated using the respective methods. The trend shows that with increasing Ti coverage, the sites become more stable.

The $TiAl_3$ alloy is a stable phase, but the formation of the bulk phase would require concentrating Ti atoms only in tiny parts of the Al grains to achieve the correct stoichiometry. The chemical potentials of different $TiAl_3$ surface terminations were calculated to complete the surface energy landscape (Figure 3). The TiAl-terminated and Ti-terminated surfaces are more stable compared to the Al-terminated surface.

Chemisorption. Our aim is to elucidate the chemisorption trends of the different surface models shown (Figure 1) above. The most energetically favorable arrangements of Ti-containing active sites will then be discussed and used to analyze the atomistic mechanism of the chemisorption of hydrogen. A more detailed description of the hydrogen chemisorption mechanism on the Model 4 surface arrangement was provided in our previous study.[14]

For studying chemisorption, different orientations of the hydrogen molecule were tested by placing the molecule in the vacuum above the surface. It was placed just within the sum of van der Waals radii of the surface atom closest to the hydrogen atoms. Dissociative chemisorption occurs for a hydrogen molecule parallel to the surface. Cases with no significant barrier for chemisorption are presented first, followed by cases with higher barriers. The Model 4 surface arrangement, which has titanium atoms as third-nearest neighbors in the unreconstructed surface, but reconstructs by shifting the row of Al atoms containing the intervening Al atom between the two Ti atoms one-half lattice position perpendicular to the Ti−Ti axis to form a rhombus-shaped active site, dissociatively chemisorbs hydrogen spontaneously. No barrier for chemisorption was observed for this model, and the chemisorbed species exhibited the lowest energy among the models with 0.25 ML coverage. The Model 4 subsurface arrangement does not reconstruct. It also promotes the dissociative chemisorption with no apparent barrier above the intrinsic endothermicity (0.26 eV) of the chemisorption reaction. The Model 3 surface arrangement, which contains second-nearest-neighbor titanium atoms, was found to dissociate molecular hydrogen with a barrier of 0.89 eV. The Model 8 surface arrangement has an activation barrier for molecular hydrogen chemisorption as high as 1.62 eV, which may explain why no catalytic activity has been reported with the bulk $TiAl_3$ alloy. The Model 3 and the vertical subsurface arrangements (Models 5−7) have apparent activation barriers for chemisorption between 1.5 and 2.5 eV. One isolated Ti atom (as shown in Model 1) exhibits only physisorption, and Model 2 appears to be inert toward even physisorption. It is indeed imperative to note that models that do not promote facile chemisorption (including pure aluminum) will chemisorb hydrogen at elevated temperatures and pressures. In this study, only those models with a range of activation barriers that are reasonable for hydrogenation of the materials under ambient conditions are considered.

Next we can examine the relative stability of the model Ti arrangements in an Al(001) surface using their chemical potentials relative to the reference state of the Ti−Al terminated surface of the $TiAl_3$ alloy. This is probably too stable a reference state because the $Ti_{0.02}Al_{0.98}$ to $Ti_{0.04}Al_{0.96}$ stoichiometry is too dilute by a factor of 8 to 16 to form more than pockets of the $TiAl_3$ alloy, so the chemical potential "barriers" to the formation of the various model active sites from the reference state are likely to be upper bounds. As shown in Table 1, the 0.5 ML subsurface site (Model 8) is lowest in energy, followed by the Model 8 surface site. From the Method 1 results, the latter is 0.61 eV/Ti atom more stable than the subsurface arrangement

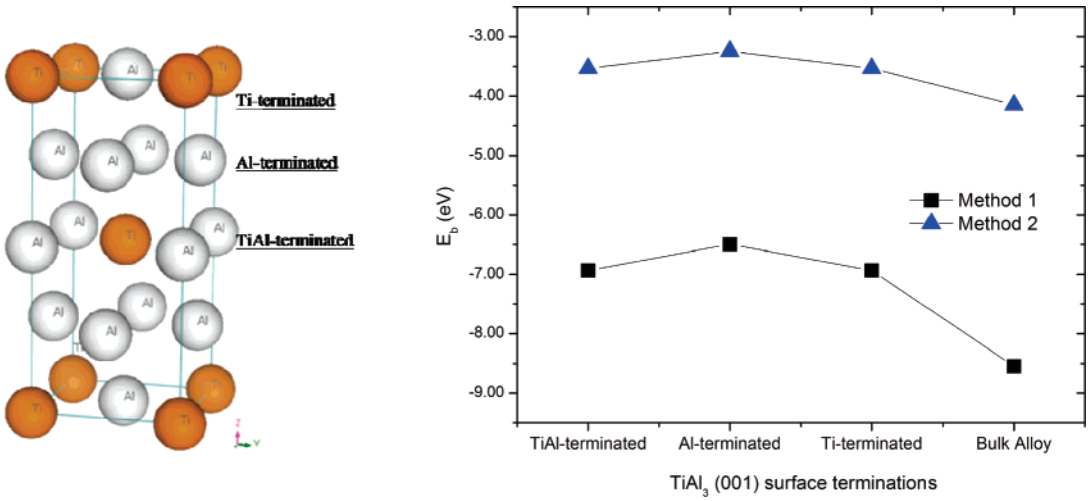

Figure 3. Three successive surface terminations possible in the stable $TiAl_3$ (001) surfaces have similar energies. The Al termination is slightly less preferred. The surface arrangement in the TiAl termination is equivalent to Model 8. The two different methods find the same trend of stability for different surface terminations.

Table 2. Combined Total Activation Energies of Probable Active Sites: Free Energies of Formation (ΔG_f)[a], Activation Energies (E_a) for Dissociative Hydrogen Chemisorption, and Their Sums[b]

property	Model 3	Model 4	Model 4s	Model 8
site ΔG_f	3.13 (0.66)	2.08 (0.59)	1.65 (0.58)	1.04 (0.36)
E_a	0.89	0.00	0.26	1.62
site $\Delta G_f + E_a$	4.02 (1.55)	2.08 (0.59)	1.91 (0.84)	2.66 (1.98)

[a] The free energies of formation in parentheses are based on Method 2 for which the differences are significantly smaller. [b] Model 4 with $\Delta G_f + E_a = 0.59$ eV becomes a more favorable site for chemisorption compared to Model 4s using Method 2, a reversal of the trend when compared to the results from Method 1.

of Model 4, the most stable 0.25 ML arrangement, and 1.04 eV/Ti atom more stable than the surface site of Model 4, the most stable 0.25 ML *surface* arrangement. This is not surprising considering it also resembles the TiAl-terminated $TiAl_3$ (001) plane (as shown in Figure 3). The surface site of Model 3 is less stable by 2.09 eV/Ti atom than the surface arrangement of Model 8. The results obtained using Method 2 order the model sites in exactly the same way, but the magnitudes of their differences are much smaller. We can now add the activation energy for dissociative hydrogen chemisorption and the (estimated) chemical potential of each promising active site to obtain an estimate of its overall efficacy (see Table 2). Because the Model 4 subsurface arrangement appears to exhibit no barrier for chemisorption in excess of its 0.26 eV endothermicity, its combined "total activation energy" using Method 1 chemical potentials is 1.91 eV, followed closely by the Model 4 surface arrangement with 2.08 eV. The Model 3 surface arrangement has a total activation energy of 4.02 eV and the Model 8 surface of 2.66 eV, both considerably higher than the Model 4 sites. Using the Method 2 chemical potentials, the order of the total activation energy of the Model 4 surface (0.59 eV) and subsurface (0.84 eV) sites is interchanged.

For surface Model 4, the H−H distance is 2.04 Å after chemisorption, and the hydrogen atoms are located above the triangular hollow sites formed by one Ti and two Al atoms. A detailed description of this reaction and chemisorbed species is provided in our previous work.[14] A Mulliken population analysis shows that the titanium atoms are oxidized during hydrogen chemisorption, and as a result, the partial charge increases from +0.29 to +0.52. The overall reaction is exothermic, and the chemisorption energy calculated with respect to the unreacted surface is −0.59 eV (−13.61 kcal/mol of H_2). The chemisorption energy for the subsurface site is slightly endothermic (5.91 kcal/mol of H_2). As documented in Table 1, the subsurface sites of Model 4 are energetically more favorable, but the surface sites are more stable after hydrogen chemisorption. Therefore, hydrogen chemisorption stabilizes the Ti atoms on the Al(001) surface more than the subsurface Ti-atoms, and thus, there can be exchange between surface Al and subsurface Ti atoms in the presence of hydrogen atoms.

Atomic orbital basis set DFT calculations using a DNP basis (as described above in the All-Electron DFT subsection under Theoretical Methods) and the same exchange-correlation functional (RPBE) have been used to study the molecular orbital description of the hydrogen chemisorption process in the catalytically active models for confirmation of the results obtained from the pseudopotential-based DFT methods. The calculations suggest an apparent nodal symmetry requirement for the most active sites. The atomic orbital basis set calculations reveal the structure of surface orbitals responsible for this symmetry requirement. Not surprisingly, the symmetry of the doped surface LUMO plays a vital part in the chemisorption process. The nodal symmetry in the surface LUMO of unreacted Model 4 is shown in Figure 4. The surface and subsurface models both have a surface LUMO with opposite phases in the out-of-plane orbital lobes that overlap with the H_2 σ^* orbital in the incipient surface-H_2 adduct. The surface Ti site has more $3d_{Z^2}$ character and the subsurface LUMO has more Al 3p character, but the basic nodal symmetry requirement is satisfied by both these frontier orbitals.

The molecular orbital interactions during the step-by-step dissociation of a hydrogen molecule reveal why the arrangements of atoms in the active sites are so important for this process. The MO diagram (shown in Figure 5) provides a simple schematic explanation for the reactivity of the Ti-doped aluminum surfaces. The energies of the surface HOMO and LUMO cross over during the adduct formation. The most interesting aspect of this result is the role of symmetry. The antibonding σ^* orbital overlaps with the unreacted surface

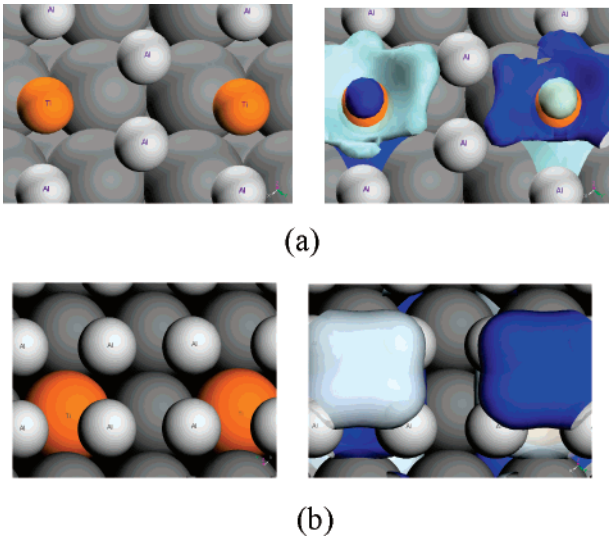

Figure 4. Arrangement of Ti atoms of the two Model 4 active sites (left frames): (a) surface and (b) subsurface. The corresponding surface LUMO that forms an adduct with the incoming H_2 molecule is also shown (right frames). The surface atoms are scaled down for better visibility of subsurface layers, and the light and dark blue colors are indicative of different phases of the molecular orbitals.

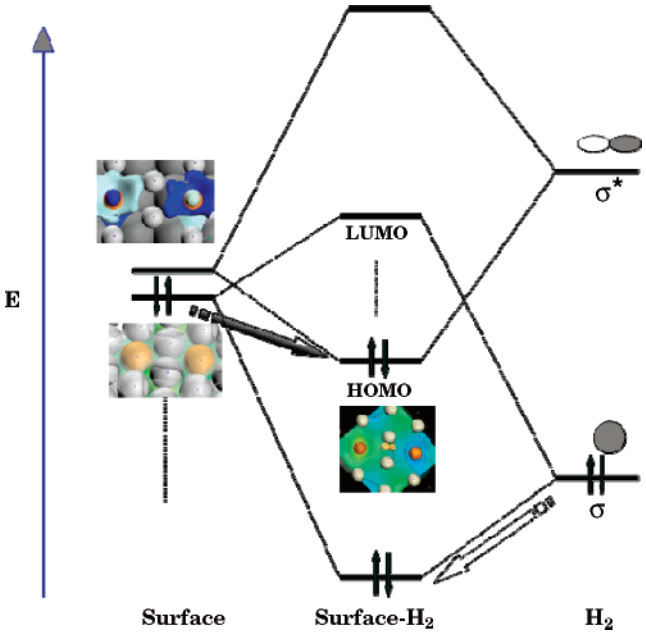

Figure 5. Molecular orbital diagram showing the symmetry controlled reaction of hydrogen atoms on a Al(001) surface.

LUMO in both the surface and subsurface sites because of the opposite phases of the orbitals normal to the surface on the two Ti atoms, and this eventually dissociates the H−H bond by transferring electron density (formally the pair of electrons in the unreacted surface HOMO) from the surface HOMO to the stabilized MO formed from the surface LUMO and σ^* orbitals.

The chemisorbed species has interesting bonding characteristics.[14] All calculations of energetics reported here, including those of the chemisorbed species, correspond to 0 K. The thermal diffusion of the energy-minimized chemisorbed hydride species was examined using density functional molecular dynamics (DFT-MD) simulations at 450 K of the Al(001) supercell with the two dissociated hydride species. Starting from the 0 K structure of the H_2 adduct, it was found that the

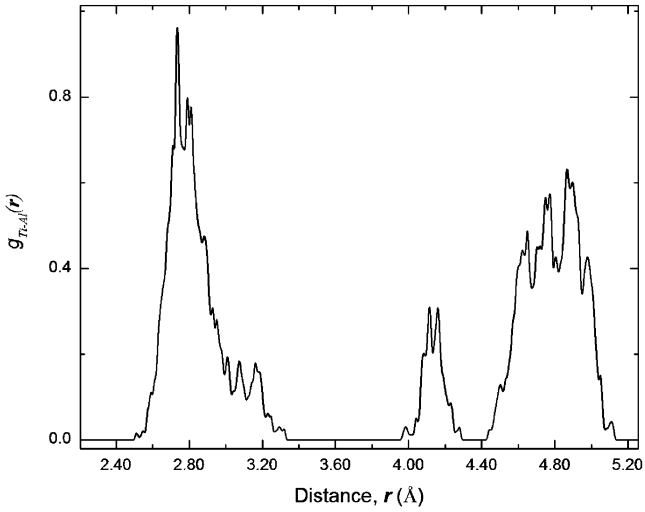

Figure 6. Distribution of Ti−Al distances from a 1 ps simulation at 450 K. The comparison with EXAFS distances is presented in the Discussion section and listed in Table 4.

dissociated hydrogen atoms can diffuse freely on the surface between adjacent triangular hollow sites consisting of two aluminum atoms and a titanium atom. Subsequent chemisorption is therefore not completely inhibited by rigid bonds with the aluminum or titanium atoms at the active site, although in the short time period of our MD simulations, no occasional diffusion to all aluminum triangular hollow sites was observed. The chemisorbed species has a high barrier to diffusion to an all-Al region on the surface (~1.57 eV), and the process is endothermic by 0.62 eV. The calculated first coordination sphere of the Ti−Al distance distribution from the 450 K simulation data (Figure 6) appears to be the sum of at least four distributions with maxima at 2.71 ± 0.02, 2.79 ± 0.02, 2.89 ± 0.04, and 3.14 ± 0.2 Å. The second set of distances around 4.11 ± 0.02 comes from the subsurface Ti−Al distances. The poor thermal averaging (1000 steps) is responsible for the noise in the Ti−Al distance distribution plot shown in Figure 6. We did not observe any recombination of the hydride species or desorption of molecular hydrogen. We anticipate this to be an unlikely scenario due to low hydride coverage and the endothermicity of the process.

Experimental Verification of Structure and Reactivity. The reverse reaction starting from the depleted material, NaH and Al, is enormously complicated to follow using X-ray absorption or diffraction or electron microscopy techniques. This is because of the highly disordered nature of the depleted material and the very small particle size owing to the evolution of hydrogen during the decomposition process. As the Ti atom plays a vital role in making the reverse reaction occur, any study of mechanism needs to separate the probable catalytic part played by Ti atoms in this amorphous mix from other solid-state reactions between the different metal hydrides. The standard way of writing the multistep reverse reaction in the presence of 2−4% Ti dopant is as follows:

$$3\ NaH + Al + 3\ H_2 \rightarrow Na_3AlH_6 \qquad (2a)$$

$$Na_3AlH_6 + 2\ Al + 3\ H_2 \rightarrow 3\ NaAlH_4 \qquad (2b)$$

The problem with this approach is the implicit assumption that titanium can catalyze reactions in either of these two steps. This

reaction can be rewritten in a way that separates the catalytic part of the reaction from the more well-known reactions of alanate formation from hydrides. Our previous calculations could not link any catalytic activity due to titanium in the sodium alanate or the cryolite phase. Similarly, the following model reactions were explored experimentally to test the hypothesis that the role of titanium is limited only to the formation of some form of aluminum hydride:

$$AlH_3 + 3\ NaH \rightarrow Na_3AlH_6 \quad (3a)$$

$$Na_3AlH_6 + 2\ AlH_3 \rightarrow 3\ NaAlH_4 \quad (3b)$$

The above reactions using bulk AlH_3 succeeded without any need of titanium doping or hydrogen gas to form sodium alanate. This is demonstrated in Figure 7a, which shows the diffraction pattern from a starting mixture of NaH and AlH_3 that was then subjected to ball milling for 18 h in an Ar atmosphere. The mechanochemical reaction produces Na_3AlH_6 (Figure 7b) and subsequently $NaAlH_4$ (Figure 7c). In the reaction proposed originally by Bogdanovic et al.,[13] the role of titanium was defined loosely as promoting the reverse reaction. The above observation supported by our computational model indicates that the role of Ti can be limited to the very first step, i.e., catalytically promoting formation of hydrides of aluminum. It may be further limited to simply catalyzing the dissociative chemisorption of molecular hydrogen.

EXAFS. The local atomic structure around the Ti atoms was investigated in hydrogenated and dehydrogenated samples at dopant concentrations of 2 and 4 mol % using EXAFS. The following results were from samples after four hydrogenation/dehydrogenation cycles under a hydrogen atmosphere using the standard procedures for experimental data reduction.[35] The k^2-weighted EXAFS ($k^2\chi(k)$) from the Ti-doped alanate and a dilute Ti−Al alloy ($Ti_{0.08}Al_{0.92}$) are shown in Figure 8a. The Fourier transform of $k^2\chi(k)$ is shown in Figure 8b, where r is corrected

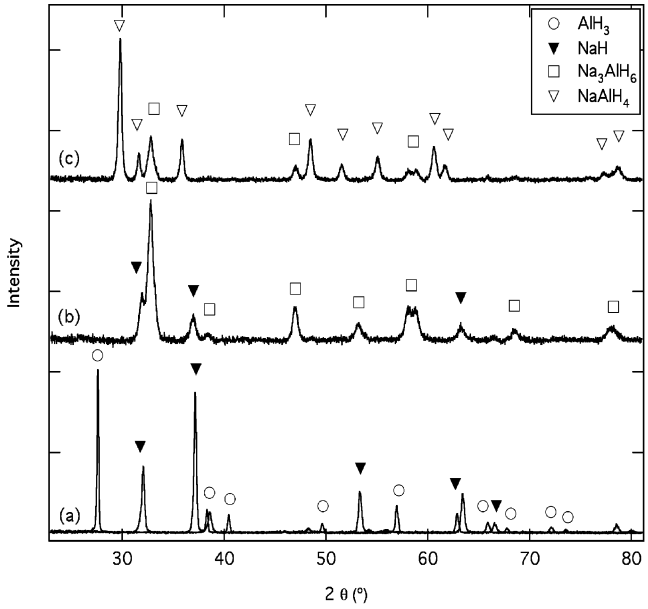

Figure 7. X-ray diffraction from (a) NaH + AlH_3 as-received (patterns are overlaid); (b) 3 NaH + AlH_3 mechanically alloyed 18 h; and (c) product from (b) + 2AlH_3 mechanically alloyed 18 h.

for the phase shift, $\delta(k)$, at the central and backscattering atoms. The dominant peak at about 2.8 Å is due to single scattering of the photoelectron by Al atoms. The more distant Ti−Ti neighbors are evident at about 3.8 Å (corrected), though these are obscured by multiple-scattering contributions to the EXAFS signal. Similar EXAFS experiments on doped alanates have shown mixed results. There is evidence that Al[17,18,34] and Ti[36] atoms are nearest neighbors to the central Ti. This discrepancy can be attributed to sample preparation. Previous studies have shown that after ball milling, the Ti is in a mixed state of $TiCl_3$ and $TiAl_3$ and in a final state of Ti−Al after 4 cycles.[18] For samples that were not cycled, or cycled only once, the Ti

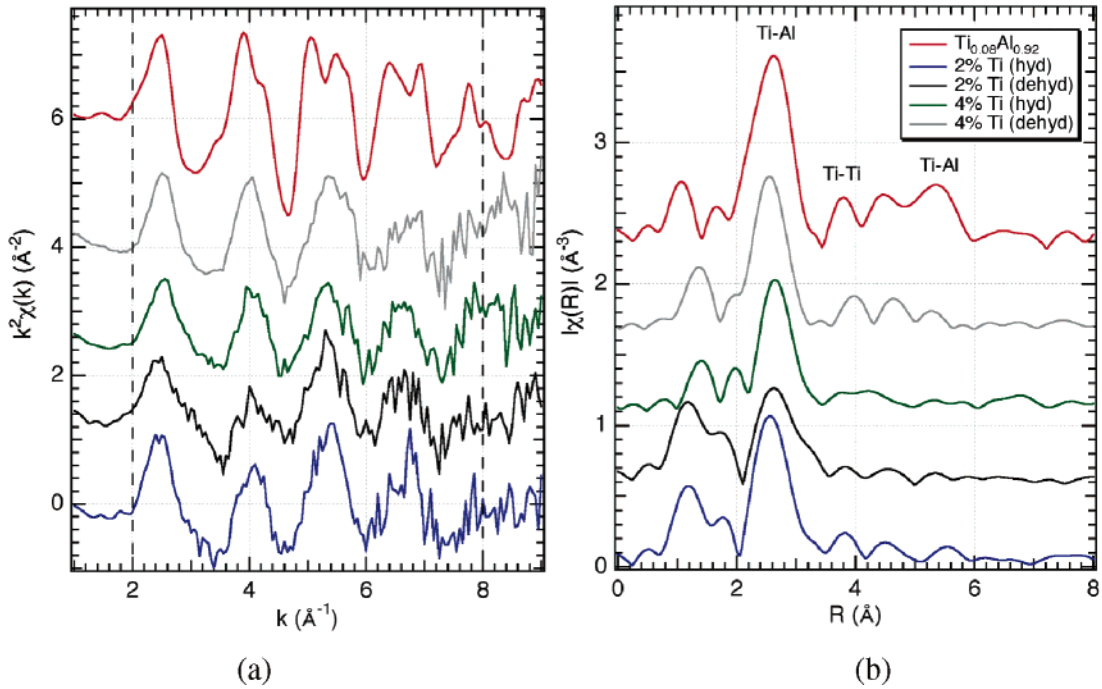

Figure 8. (a) k^2-weighted EXAFS data of a dilute Ti−Al alloy ($Ti_{0.08}Al_{0.92}$) and other 2−4% titanium-doped sodium alanate samples at the end of hydrogenation-dehydrogenation cycles. (b) Fourier transform of the k^2-weighted EXAFS data showing the local Ti coordination.

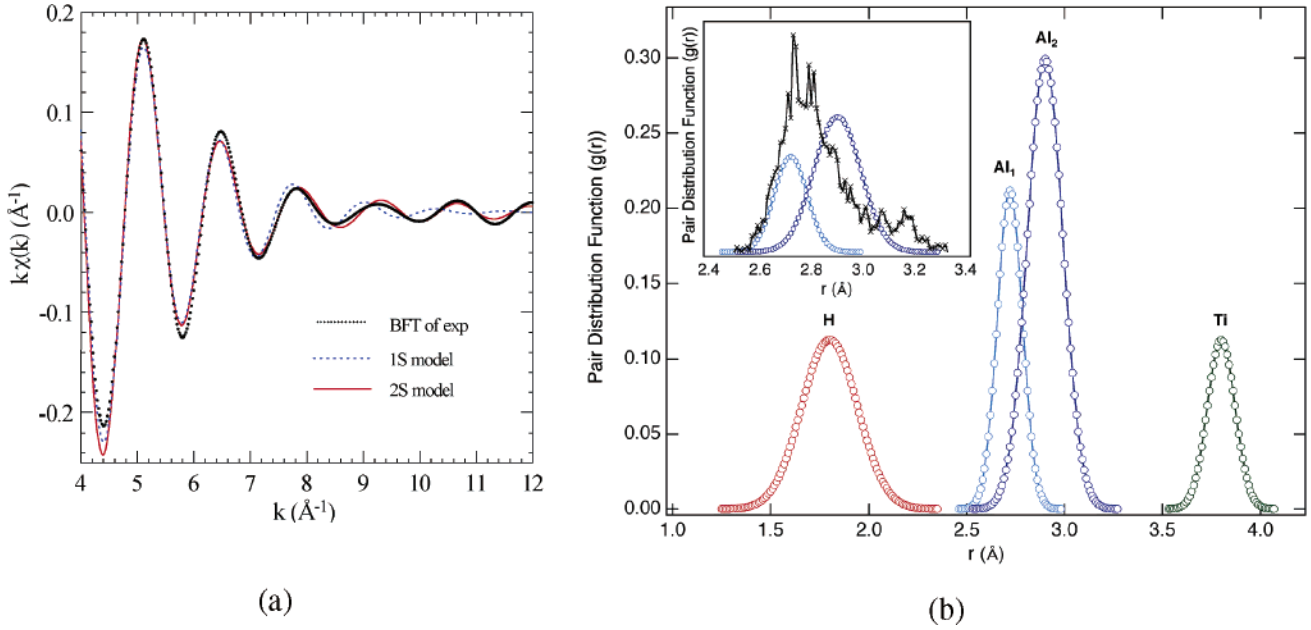

Figure 9. (a) Back Fourier transform of experimental data and experimental fits using 1S (cubic, *Pmm*) and 2S (tetragonal, *I*4/*mmm*) models. (b) Pair distribution function calculated from EXAFS data on 2 mol % Ti-doped $NaAlH_4$ (hydrogenated) and corrected for the phase shift. (Inset) Comparison of the predicted and experimental distribution functions for the Ti−Al pairs.

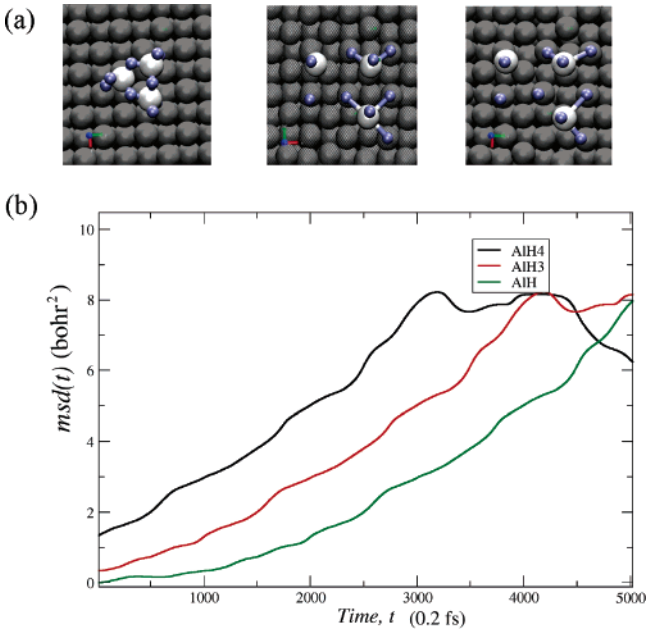

Figure 10. (a) Dissociation and diffusion of the Al_3H_9 cluster on an Al-(001) surface showing formation of smaller fragments including a stable AlH_4 and AlH_3 cluster; (b) mean-square displacements of the fragments from a 10 ps Car-Parinello simulation of the Al_3H_9 cluster on Al(001). The AlH_4 cluster ultimately disintegrates into smaller fragments contributing to the apparent saturation effect shown by the mean square displacement for AlH_4.

remains in an intermediate state, possibly surrounded by Ti atoms, which ultimately progresses to the more stable Ti−Al state with cycling.

The *k*-weighted EXAFS from the Ti−Al pairs was isolated through a back Fourier transform to *k* space (Figure 10a). The data were fit to two competing models using one-site (1S) and two-site (2S) Ti−Al Gaussian pair distributions. The 2S model was further constrained to six structural parameters: short and long Ti−Al distances (R_1 and R_2), two corresponding Debye−Waller (DW) factors, number of short-distance neighbor (N_1) (whereas $N_2 = 2{*}N_1$), and one energy shift, ΔE. The 1S model utilized the standard set of the structural parameters (*R*, DW, *N*, and ΔE). The amplitudes and phase shifts were generated by the FEFF7 code.[37] Both models provide good agreement (R_a-(2S) = 7.6 and R_a(2S) = 6.0) for values of $k < 8$ Å^{-1}, whereas only the 2S model fits the data at higher *k*. Therefore, two different Ti−Al distances are present, suggesting a tetragonal (*I*4/*mmm*) local symmetry for the first shell.

The structural parameters, based on the tetragonal model, are summarized in Table 3. The central Ti atom is coordinated by a split shell of Al atoms at approximately 2.72 and 2.90 Å, consisting of 3.4 and 6.8 atoms, respectively. These coordination numbers are reduced compared with the expected 4 and 8 from perfect tetragonal symmetry. Similarly, the Ti neighbor at 3.8 Å consists of only 2 atoms, which is approximately half the expected value for the *I*4/*mmm* phase of $TiAl_3$. The reduced coordination numbers suggest that the central Ti atom is located on or near (within a monolayer) the surface.

The pair distribution function (corrected for $\delta(k)$, shown in Figure 9b) was calculated from the following equation:

$$g(r) = \sum_i \frac{N_i}{(2\pi)^{1/2}} \exp[-(r - R_i)^2/2\sigma_i^2] \qquad (4)$$

where N_i, R_i, and σ_i are the coordination number, distance, and Debye−Waller factor for the *i*th neighbor, respectively. The number of atoms in each shell is reflected in the integrated intensity. The peak width represents the relative displacement of the Ti−X pair. The small features around 1.8 Å in the EXAFS signal (Figure 9b) may be indicative of four loosely bound H atoms. However, it should be noted that due to the small cross

(35) Hayes, T. M.; Boyce, J. B. *Solid State Physics*; Academic Press: New York, 1982; Vol. 37, p 173.
(36) Leon, A.; Kircher, O.; Rothe, J.; Fichtner, M. *J. Phys. Chem. B* **2004**, *108*, 16372.
(37) Zabinsky, S. I.; Rehr, J. J.; Ankudinov, A.; Albers, R. C.; Eller, M. J. *Phys. Rev. B: Condens. Matter Mater. Phys.* **1995**, *52*, 2995.

Table 3. Local Structure Parameters for $TiAl_3$ and 2 Mol % Ti-Doped $NaAlH_4$ Including Interatomic Distance (R), Debye−Waller Factor (DW), and Coordination Number (N)[a]

	$NaAlH_4$ + 2% Ti			$TiAl_3$		
	Al_1	Al_2	Ti	Al_1	Al_2	Ti
R (Å)	2.72 ± 0.02	2.90 ± 0.02	3.80 ± 0.03	2.74 ± 0.02	2.88 ± 0.02	3.84 ± 0.04
N	3.4 ± 0.5	6.8 ± 1.0	2.0 ± 1.0	3.8 ± 0.4	7.6 ± 1.0	4
DW × 10^{-3} Å^2	4.1 ± 0.8	8.2 ± 1.2	5.2 ± 1.5	3.7 ± 0.6	6.7 ± 1.0	−

[a] All values are based on model using a tetragonal unit cell in the *I*4/*mmm* space group (split Al shell). The fit is shown in Figure 9a

Table 4. Comparison of Distances[a] of Different Relevant Arrangements from Experimental EXAFS and DFT Calculations[b]

	Ti oxidation state[17]		Ti–Ti distance (Å)			Ti–Al distance (Å)		
condition	expt.	theory	expt.	theory		expt.	theory	
hyd.				2.72	Model 2		2.69	Model 8
	0.17	0.37	3.8	3.79	Model 8	2.72	2.71	Model 4s
				4.05	Model 3		2.76	Model 3,8
				5.14	Model 4s		2.80	Model 4
				5.43	Model 4	2.90	2.89	Model 3,4,8
							4.72	Model 4
dehy.				2.72	Model 2	2.72	2.71	Model 4
	0.36	0.52	3.8	3.79	Model 8		2.69	Model 8
				4.43	Model 3		2.80	Model 3
				5.17	Model 4s	2.90	2.89	Model 3,4,8
				5.40	Model 4		4.76	Model 4

[a] The calculated distances are from the four overall most energetically favorable sites: Model 4 surface, Model 4 subsurface, Model 8 surface and Model 3 surface. [b] The distances for the hydrogenated sample in the case of theory are from the unreacted surface, and the dehydrogenated distances are from the surface with the chemisorbed hydrogen. Model Xs means the subsurface site of Model X.

section of H, it is difficult to definitively determine the number of H neighbors. A comparison of the experimental and the theoretical pair distribution functions is shown as an inset in Figure 9b. The differences in intensity can be attributed at least in part to the fact that the DFT-MD simulations were carried out for the hydrogenated Model 4 surface only, and the physical material is a complex mixture of many such possible environments (as the calculated distances show in Table 4) including regions that resemble the $TiAl_3$ alloy locally.

4. Discussion

The above results illustrate the complicated way in which the reverse reaction, i.e., the hydrogen storage reaction, proceeds. The experimental results can be summarized as: (a) bulk AlH_3 will react with NaH to form sodium alanate and (b) Ti environments detectable in EXAFS are all from the metallic Al phase. The EXAFS results also provide the following framework for theoretical modeling: (1) The Ti atoms are located in the metallic Al phase and the Ti−Al coordination environment does not change during the hydrogenation reaction. The plot in Figure 8 shows that there is a broad distribution of distances in this highly disordered sample, and the overall Ti−Al and Ti−Ti distances do not show any significant shift during the hydrogenation−dehydrogenation cycles; (2) the catalytic effect of Ti can be limited to activating aluminum for hydrogen chemisorption, and perhaps catalyzing aluminum hydride formation. The theoretical modeling adds further detail about the arrangements that are possible for the Ti atoms. First, subsurface Ti atom arrangements are thermodynamically favored in the absence of hydrogen. Interestingly, the chemisorbed species at the Model 4 active sites makes the surface arrangement more stable. It is important to compare the Ti−Al and Ti−Ti distances that are available from the pair distribution functions calculated from EXAFS (Figure 9) and computational models. The surface models are highly idealized (i.e., flat and periodic) compared to many conceivable variations of the Al surface which include different microfacets, vacancies, adatoms, steps, and edges, but it is nevertheless important to look for features common to the experimental and theoretical results and to attempt to understand any discrepancies between them. The EXAFS model shows a very high degree of disorder beyond 4 Å in radial distance from a Ti atom. Conversely, the periodic surface model is ordered and the peak widths arise mainly through thermal vibrations averaged over a very short period of time (1 ps) as calculated from multiple trajectories of DFT-MD simulations of the surface after chemisorption. With this caveat in mind, the simulated and experimental distances are in generally good agreement (as shown in Table 4). The difference between the intensities of the experimental and calculated distribution functions is at least in part the result of: (a) there being a significant difference between the small simulated supercell vs. the highly disordered depleted material with only regions of Ti-containing areas resembling our model systems, and (b) our pdf being only from a simulation of our chemisorbed Model 4 surface, one of the many possible model systems we have studied. The distances above 4 Å listed in the Table 4 are hard to resolve in the experimental data. The broad nature of the peaks between 4 and 6 Å could simply be owing to broad and overlapping intensities from similarly spaced Ti−Al and Ti−Ti coordination environments in the radial distribution plots (Figure 8).

The two sets of Ti−Al distances seen at 2.72 and 2.9 Å are possible from Model 4 (Figure 4) alone depending on the surface or subsurface arrangement of Ti atoms. Surface Model 4 reconstructs to form the rhombus described before and prefers a longer (2.89 ± 0.3 Å) Ti−Al distance compared to the subsurface model (2.71 ± 0.3 Å). The shorter distance can also be from higher than 0.25 ML Ti coverage of aluminum surfaces, as exhibited by Model 8. The Ti−Ti distances are more complicated, as many of the Ti−Ti distances seen in the computational models are in the region that is hard to refine from the EXAFS data. The only Ti−Ti distance seen in EXAFS is 3.8 ± 0.03 Å. The calculated distances are 4.3 Å for Model 3 followed by 4.9 Å in the unreconstructed subsurface Model 4 (refer to Figure 3). The 3.8 ± 0.03 Å distance is only possible if the 0.5 ML coverage (shown in Model 8) is present as a surface or subsurface phase. The question that remains harder to answer is: Which distance between Ti atoms is responsible for catalyzing the chemisorption process? It is not possible to determine the catalytic activity of a Ti−Ti pair from EXAFS results. The all-electron DFT results point to the importance of nodal symmetry and thus suggest that the arrangement of the pair of Ti atoms is critical. However, the doped aluminum surface at 0.5 ML of Ti coverage, which has a Ti−Ti distance of 3.8 Å, has a higher activation barrier for hydrogen chemi-

sorption compared to the 0.25 ML sites that satisfy the nodal symmetry requirement discussed before. The EXAFS data show that as much as 50−75% of the Ti atoms can be located at the short distance of 3.8 Å in the dehydrogenated sample. Still, it is hard to conclude that the remainder of the Ti atoms will not find the thermodynamic minimum during multiple hydrogenation−dehydrogenation cycles. (Please refer to the Figure S1 in the Supporting Information, which shows the chemical potential of all the model sites in the order of increasing stability in eV/atom.)

An important unresolved question (and one that is unlikely to have a unique answer) is: Which site is primarily responsible for the chemisorption? In an attempt to answer this question, a number of different possible environments were investigated, and each was evaluated for viability as an active site according to the sum of its chemical potential (relative to the reference state corresponding to the most stable arrangement of the system) and its activation energy for dissociatively chemisorbing molecular hydrogen (these sums are listed in Table 2). The results suggest that the lowest-energy site may not be the most active site. For example, the 0.5 ML surface coverage by titanium (Model 8) is the most stable of the set of potential active sites we studied, but the sum of the chemical potential (see Table 1) and the activation barrier (nearly 1.62 eV for the surface site, higher still for the subsurface site) will place these sites considerably higher in overall activation energy than the best of the 0.25 ML sites. The Model 4 subsurface and surface sites are more likely to be major participants in the chemisorption process. The scenario is further complicated by the stabilization of the surfaces by the presence of atomic hydrogen in the system, especially during the hydrogenation reaction. It can change the ordering of stability of the active sites as well; the chemisorbed hydrogen atoms stabilize the titanium atoms on the surface layer. For example, a subsurface 3rd-nearest-neighbor titanium-containing site is more stable by 0.43 eV/atom compared to the analogous surface site. The surface site gains ∼0.59 eV in stability in the presence of chemisorbed hydrogen atoms, whereas the subsurface site becomes less stable by ∼0.26 eV. As a result, the presence of hydrogen atoms can possibly promote an exchange between surface aluminum atoms and the subsurface titanium atoms. The overall picture is thus highly dynamic, but the results of both Method 1 and Method 2 calculations of the chemical potentials indicate that a significant role for Models 4 and 4s in the chemisorption process is expected. At any point in time during the reaction, there are various nonequilibrium processes occurring. These include surface/subsurface exchange, surface and bulk diffusion, physisorption, chemisorption, and nucleation of new phases, all of which can simultaneously contribute to the overall catalytic activity.

The comparison of the EXAFS and the theoretical interatomic distances (Table 4) is problematic because the overlap of the 2nd Ti−Al peak and higher-order Ti−Ti peaks in the radial distribution function (5−6 Å) makes it difficult to quantify the coordination numbers at these sites. Our experimental results indicate that with multiple cycling, the system becomes more ordered, i.e., sites resembling $TiAl_3$ arrangements start forming and reduce the catalytic activity of the system. Other experimental evidence supporting that observation has started to come forward from some diffraction studies; Haiduc et al. also confirmed the presence of Al_xTi-intermetallics and indicated that the catalytic activity is lower with more ordered phases resembling $TiAl_3$.[38]

Diffusion of Alane. Finally we can discuss the possible fate of the surface hydride species (AlH_x) that manages to form on the aluminum surface. The diffusion of this aluminum hydride species to the NaH phase represents the final piece of the puzzle that needs to fall into place. We have shown that bulk AlH_3 itself will form sodium alanate albeit slowly in a ball milling experiment with NaH. At much lower temperatures, Reutt-Robey et al.[21] have experimentally showed the existence of alane clusters when an Al(111) surface was exposed to atomic hydrogen. All these molecular clusters such as AlH_3 and Al_2H_6 are stable in the gas phase. We therefore tried to answer the following questions: (a) Are these clusters stable enough to survive at the operating temperature of the hydrogen storage reactions? and (b) Is their diffusion rate sufficient to provide a constant supply of reactants to the NaH grains? (Once the clusters are delivered to NaH, nucleation of the Na_3AlH_6 phase should be even easier than in our experimental setup, where some energy is required to break the bulk AlH_3 lattice.)

We used Car−Parinello (CP) MD simulations as described in the Theoretical Methods section to investigate different alane clusters placed on an Al(001) surface at different temperatures and at longer time and length scales than we could treat with the CASTEP program. The simulation results were then analyzed for the stability and the diffusion rate of the clusters. The results indicate that the transport is unlikely to occur with the larger clusters, since both Al_2H_6 and Al_3H_9 break down to AlH_3 (and $AlH_x + H$) on Al(001) as shown in Figure 10. The smaller AlH_3 clusters, along with other fragments such as AlH_2, AlH, and H, are stable in 200 and 400 K simulations. A single AlH_3 cluster created by the breakup of Al_3H_9 was observed to survive through three sequential restarts of CPMD trajectories of 5−10 ps without further fragmentation. These CP results imply that the aluminum species that carries the hydrogen is most likely the smaller clusters (AlH_x where $x \leq 3$) with high diffusion rate driven by the thermal vibrations. Although first-principles theory predicts stable cyclic hydrogen-containing clusters in the gas phase, it is evident that AlH_3, with an approximate diffusion rate of 3×10^5 cm/sec, is the most probable cluster among the alanes for participation in the mass transport. It is hard to predict if the formation and the diffusion of the alane species are rate limiting. The low-temperature experiments show[21] that Al atoms are extracted preferentially from step edges and hence provide a clue about how an Al surface can be etched away to form alane clusters. If the formation of alanes from aluminum surfaces starts from step edges, it is likely that the control of surface morphology and particle size of the aluminum phase through optimization of reaction conditions would have a significant impact on the rate of the reverse reaction.

5. Conclusions

The complicated inorganic solid-state reaction involving dehydrogenation/rehydrogenation of sodium alanate has been studied using multiple complementary experimental and theoretical methods. The use of multiple techniques has led to the

(38) Haiduc, A. G.; Stil, H. A.; Schwarz, M. A.; Paulus, P.; Geerlings, J. J. C. *J. Alloys Compd.* **2005**, *393*, 252.

identification of important steps and has allowed each such step to be studied in isolation. The inclusion of theoretical results provides atomistic detail valuable for interpreting the experimental results and aiding the analysis of the mechanism of the chemical processes responsible for hydrogen storage in sodium alanate.

Using the combined EXAFS and density functional theory techniques, we have attempted to investigate three issues that are the most critical for understanding the hydrogen storage reactions: (a) the role of titanium in catalytic dissociative chemisorption of molecular hydrogen—the first step that allows this reaction to occur under relatively mild conditions; (b) the structural details regarding the arrangement of probable active sites and the ordering of configurations with respect to the titanium−aluminum chemical potential landscape; and (c) the formation and diffusion of aluminum hydride (e.g., alane) as the means for the transport of aluminum and hydrogen to NaH grains for subsequent reactions. The conclusions reached here are as follows: (a) titanium, located on or near the surface, indeed catalyzes the dissociative chemisorption of molecular hydrogen on an aluminum surface by lowering the activation barrier; (b) there may be multiple active sites with negligible barriers for chemisorption that can contribute to the catalytic activity, but the nodal symmetry of a frontier molecular orbital at the active site involving at least two Ti atoms appears to play a vital role in promoting charge transfer from the surface to the molecular hydrogen; (c) although we have not provided a definitive mechanism for the formation of alanes, the AlH_3 cluster has been shown to be a stable and mobile species on an aluminum surface. In addition, we have provided the first evidence that demonstrates that aluminum hydride can drive the overall reaction to form sodium alanate in the absence of titanium.

It is likely that in this dilute system with only 2−4 mol % titanium, the chemistry is very much a local phenomenon dominated by changes in the potential energy surface near the dilute or impurity atoms. This dilute nature of the sample may also give rise to multiple sites that can simultaneously contribute to the overall reactivity. The diffusion of aluminum hydride clusters suggested here has yet to be observed experimentally, but we have provided molecular-dynamics-based evidence in support of such a model. On the experimental side, we have used AlH_3 to drive the reaction with a NaH lattice to form first Na_3AlH_6 and then $NaAlH_4$ without the use of titanium as a catalyst or the presence of molecular hydrogen. The focus of our ongoing effort will be to identify the aluminum hydride species responsible for mass transport using more direct methods under controlled conditions.

Acknowledgment. This work was performed at Brookhaven National Laboratory (BNL) under Contract No. DE-AC02-98CH10886 with the U.S. Department of Energy and supported by it Division of Chemical Sciences, Office of Basic Energy Sciences. Additional support was provided by BNL's Center for Functional Nanomaterials (CFN), a BNL LDRD (No. 05-021) award, and a DOE BES Hydrogen Fuel Initiative award (BO-130). S.C. and J.T.M. gratefully acknowledge useful discussions with Roland Stumpf, regarding the chemical potential of reference states, and general discussions with Peter Sutter, Duane Johnson, and Robert Hwang. This manuscript has been authored by Brookhaven Science Associates, LLC.

Supporting Information Available: Plot (Figure S1) showing the trend of relative stability of all the model sites is included. This material is available free of charge via the Internet at http://pubs.acs.org.

JA060437S